THE SKELETAL PHENOTYPE OF THE KK/AY MURINE MODEL OF TYPE 2 DIABETES

by

Nusaiba Nahola Chowdhury

A Thesis

Submitted to the Faculty of Purdue University

In Partial Fulfillment of the Requirements for the degree of

Master of Science in Biomedical Engineering

Department of Biomedical Engineering at IUPUI

Indianapolis, Indiana

August 2022

THE PURDUE UNIVERSITY GRADUATE SCHOOL
STATEMENT OF COMMITTEE APPROVAL

Dr. Joseph M. Wallace, Chair
Department of Biomedical Engineering

Dr. Matthew R. Allen
Department of Anatomy, Cell Biology, and Physiology
Indiana University School of Medicine

Dr. Robert N. Bone
Department of Pediatrics
Indiana University School of Medicine

Dr. Sungsoo Na
Department of Biomedical Engineering

Approved by:
Dr. Joseph M. Wallace

TABLE OF CONTENTS

LIST OF TABLES

LIST OF FIGURES

LIST OF ABBREVIATIONS

T2D	Type 2 Diabetes
T1D	Type 1 Diabetes
GLUT-2	Glucose Transporter-2
AGEs	Advanced Glycation End-Products
ROS	Reactive Oxidative Species
TNF	Tumor Necrosis Factor
CKD	Chronic Kidney Disease
GFR	Glomerular Filtration Rate
ACR	Urinary Albumin/Creatinine Ratio
eNOS	Endothelial Nitric Oxide Synthase
BMD	Bone Mineral Density
PTH	Parathyroid Hormone
FGF23	Fibroblast Growth Factor 23
HbA1c	Glycated Hemoglobin
IACUC	Institutional Animal Care and Use Committee
GTT	Glucose Tolerance Test
ITT	Insulin Tolerance Test
AUC	Area Under the Curve

ABSTRACT

Type-2-diabetes (T2D) is a progressive metabolic disease characterized by insulin resistance and β-cell dysfunction leading to persistent hyperglycemia. It is a multisystem disease that causes deterioration of multiple organ systems and obesity. Of interest, T2D affects the urinary system and is the leading cause of kidney disease. Both T2D and chronic kidney negatively impacts the skeletal system and increases fracture incidence in patients. Therefore, it is important to establish an animal model that captures the complex multiorgan effects that is common in T2D. In this study, we characterized the metabolic phenotype of the KK/Ay mouse model, a polygenic mutation model of T2D. We concluded that KK/Ay mice closely mimic T2D and are hyperglycemic, hyperinsulinemic and insulin resistant. KK/Ay mice have also had worsened kidney function as supported by elevated levels of blood urea nitrogen, phosphorous, creatinine, and calcium in plasma exhibiting the kidney's inefficiency in clearing waste from the body. Even though we were able to confirm a metabolic phenotype for T2D and diabetic nephropathy, the skeletal effects of the disease were minimal and major differences in bone physiology were driven by sex differences. This study offered valuable insight into preliminary endpoints for the KK/Ay mouse mode that will decide the direction for future use of this model. We plan to use older mice in future studies to allow a longer time for skeletal effects to more prominently manifest.

1. INTRODUCTION

Diabetes mellitus is a worldwide epidemic with 462 million patients diagnosed and another 193 million individuals potentially undiagnosed[1]. Diabetes mellitus is a complex metabolic disorder that is marked by hyperglycemia, a condition in which individuals have physiologically elevated blood glucose levels [2]. Diabetes is a multisystem disease and is associated with several comorbidities including coronary heart disease, chronic kidney disease, hypertension, depression, thyroid gland diseases, and chronic obstructive pulmonary diseases, with prevalence of multiple comorbidities increasing with increasing age [3].

The pathogenesis of diabetes commonly classifies diabetes into two major categories. Type-1 diabetes (T1D) constitutes about 5-10% of patients with diabetes mellitus in which autoimmune destruction of the insulin-producing pancreatic β-cells causes insulin deficiency and hyperglycemia. Type-2 diabetes (T2D) is more prevalent and constitutes about 90-95% of all diabetes cases and hyperglycemia is a result of insulin resistance and β-cell dysfunction[2]. Obesity, defined by a body mass index of greater than 26kg/m^2, is prevalent in both T1D and T2D with approximately 55% of T1D and 86% of T2D patient being overweight or obese[4].

Insulin and glucagon, produced by islet cells within the pancreas, work antagonistically to regulate blood glucose levels. Insulin, produced by β-cells, stimulates cells to increase their glucose uptake when blood glucose levels are high. Glucagon, produced by α-cells in the pancreas, stimulates the breakdown of glycogen into glucose which is then released into the bloodstream [5]. In healthy individuals, β-cells take in glucose through the glucose transporter proteins in response to insulin, and initiates the breakdown to glucose to produce ATP[6]. The ATP concentration increases and closes the ATP-dependent potassium ion (K^+) channel on the cell membrane. This inhibition depolarizes the plasma membrane and causes the voltage dependent calcium ion (Ca^{2+}) channel to open. Calcium ion concentration increases with the β-cells, which causes the exocytosis of preformed vesicles, thereby, stimulating insulin secretion from the cell. The insulin then act on the circulating glucose within the blood [6, 7] (**Fig. 1A**). Insulin then stimulates cell of other tissues to uptake glucose to be stored as glycogen or converted to fat[5].

Diabetes mellitus is the result of elevated blood glucose levels due to dysregulation of insulin secretion or action[5]. In individuals with T1D, autoantibodies targets β-cells and causes cell death. This results in severe insulin deficiency over the progression of the disease and therefore

affected individuals become severely hyperglycemic. In individuals with T2D, hyperglycemia is a result of either insulin resistance or β-cell dysfunction. Insulin resistance occurs when peripheral tissues, such as muscle cells, liver cells, and adipose tissue have dysfunctional insulin receptors causing reduced insulin response.[2]. Insulin resistance is T2D is caused by several factors including free fatty acids secreted by adipocytes and hyperglycemia itself [6]. This reduced insulin sensitivity triggers the pancreatic β-cells to overproduce insulin as a compensatory response to prevent hyperglycemia, resulting in elevated circulating insulin levels in blood, a condition known as hyperinsulinemia. Over the progression of T2D, the β-cells become stressed and initiate apoptotic pathways, resulting in insulin deficiency[2]. Hyperglycemia induces cellular stress which glycates proteins and forms advanced glycation end products (AGEs). Obesity, hyperglycemia, and hyperlipidemia also generate reactive oxidative species (ROS) which cause oxidative stress in β-cells. Overproduction of ROS causes macrophages in adipose tissue to release more cytokines, such as tumor necrosis factor (TNF). This increases systemic inflammation and contributes to insulin resistance[8]. The ROS generated inhibits Ca^{2+} mobilization, activates proapoptotic signals and degrades insulin precursors (**Fig. 1B**). The physiological defect in insulin precursors or insulin leads to insulin secretory dysfunction and is the primary driver of β-cells dysfunction and the pathogenesis of T2D [7].

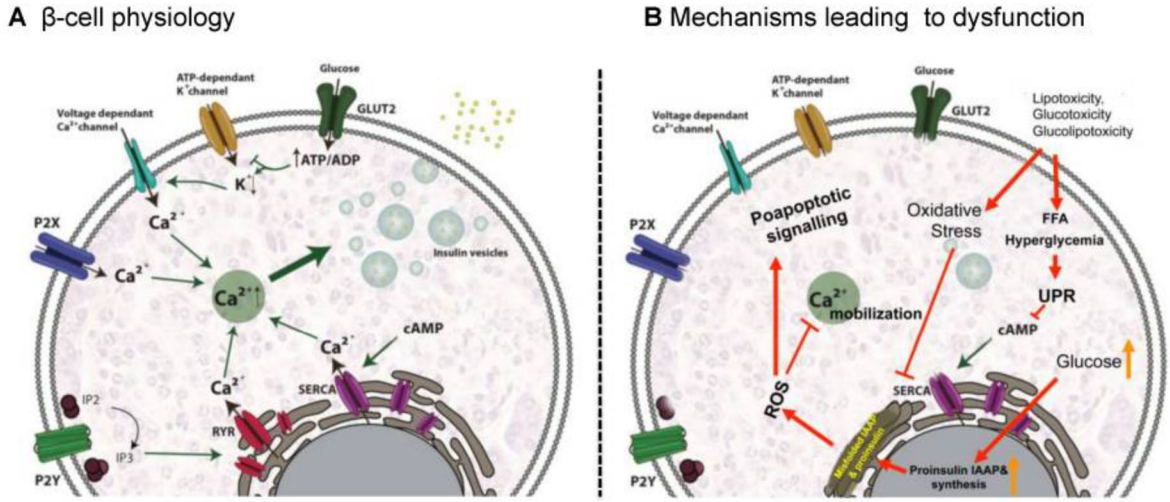

Figure 1: (A) Beta-cell physiology in healthy individuals **(B)** Beta-cell dysfunction mechanism.[7]

Chronic kidney disease (CKD) affects approximately 13.4% of the global population, and diabetes is the leading cause of CKD worldwide [9, 10]. CKD is a progressive disease marked by

loss of renal function and elevated albumin excretion. As renal function worsens, the kidney's ability to filter blood and clear waste deteriorates making dialysis or kidney transplant a necessity over the progression of the disease to prevent azotemia, systemic organ damage, and death [11, 12]. Serum creatinine levels are used to calculate glomerular filtration rate (GFR), and urinary albumin/creatinine ratio (ACR) is used to detect proteinuria. In CDK, ACR is greater than 30mg/g and GFR is less than 60ml/min/1.73 m^2. When GFR levels fall below 15ml/min min/1.73 m^2 the patient has reached end-stage kidney failure [12, 13]. The pathogenesis of kidney disease reducing GFR is due to structural, physiological, hemodynamic, and inflammatory processes. Early changes to kidney function are marked by glomerular hyperfiltration and hypertrophy. The glomerular basement membrane thickens, mesangial matrix accumulates, and nodular glomerulosclerosis develops leading to increased excretion of urinary albumin and progression of kidney disease[14].

CKD affects half of the individuals with T2D and one-third of individuals with T1D, and predominant factors include hyperglycemia and hypertension [14, 15]. Hyperglycemia is the major driver of nephropathy in diabetic patients and leads to kidney disease by altering multiple biochemical pathways within the kidney (**Fig. 2**) [14]. On a cellular level, hyperglycemia affects renal cell and β-cell dysfunction in a similar fashion. Hyperglycemia hyperactivates protein kinase C, overproducing ROS causing oxidative stress [11] . High glucose levels also prevents the generation of glutathione, a critical antioxidant, and further increases oxidative stress[14]. In its early stages, hyperglycemia increases endothelial nitric oxide synthase (eNOS) in the afferent arterioles and glomerular capillaries of the nephron. This leads to vasodilation and increases GFR. Over its progression, glomerular distension causes endothelial dysfunction and hemodynamic alterations. Thickening of glomerular basement membrane, decreased number of podocytes, and mesangial expansion triggers the initial glomerulosclerosis. Elevated ACR due to thickened glomerular basement membrane causes renal tubular cells to produce mediators, proinflammatory cytokines, and growth factors. Protein glycosylation and AGE increase activates AGE receptors in the kidney and produces inflammatory cytokines and growth factors [14]. These factors exacerbate proteinuria and activate tubular cell death. Macroangiopathy, i.e., thickening of capillaries due to diabetes, results in reduced blood flow to the peritubular capillaries. Renal function and structure impairment spreads throughout the glomerulus leading to focal and segmental glomerulosclerosis. Glomerular injury causes tubular damage and eventually tubular cell death, cell infiltration, tubule degeneration, and interstitial fibrosis [14].

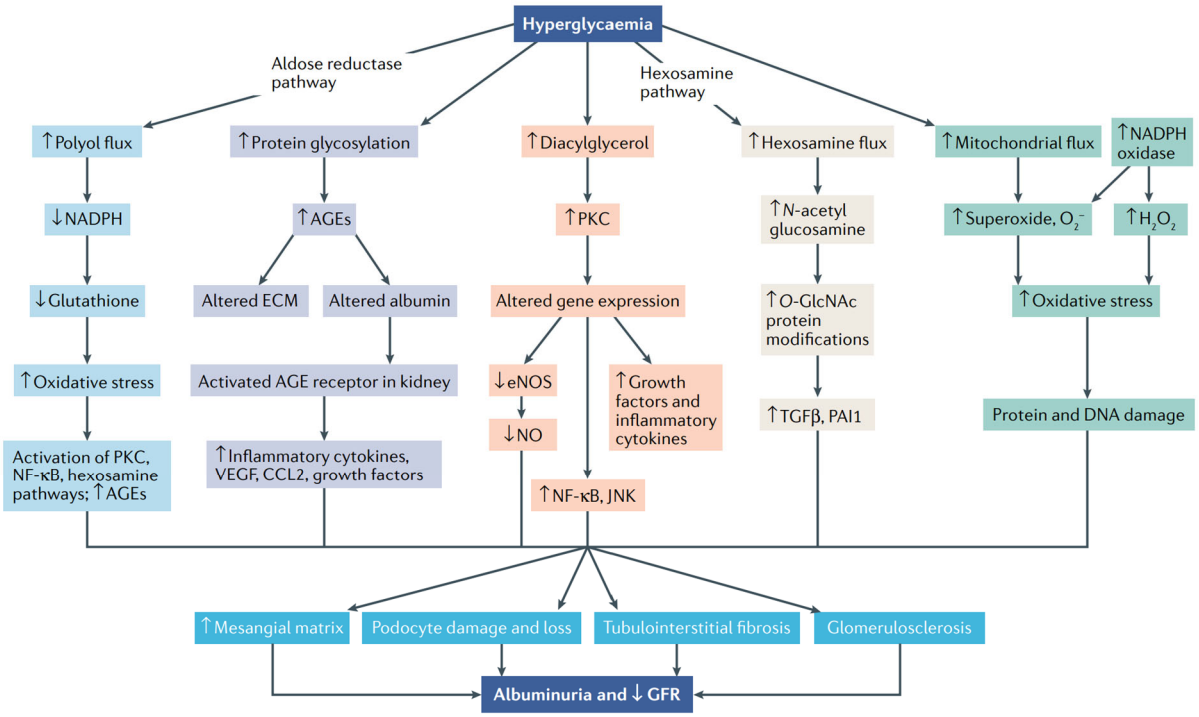

Figure 2: Effects of hyperglycemia on kidney. [14]

Skeletal fractures are a significant comorbidity in diabetes mellitus. Hyperglycemia generates increased inflammation, and overproduction of ROS and AGEs. These factors, in combination with reduced insulin signaling, increases the ratio of RANKL/OPG and causes osteoclastogenesis. Bone resorption therefore increases as more bone-resorbing osteoclasts are formed [8]. Simultaneously, expression of factors that stimulate osteoblasts such as BMPs and growth factors decrease which reduces osteoblast formation and induces osteoblast apoptosis. Bone formation and bone quality decrease as bone-forming osteoblasts decrease in number [8] (**Fig. 3**). Typically, a decrease in bone mineral density (BMD) is associated with increased skeletal fractures. This stands true for T1D individuals, however in T2D, patients have higher skeletal fractures despite having a higher BMD [8, 16]. Therefore, intrinsic bone architecture may be compromised in T2D affecting bone cell function and causing fractures at lower stress.

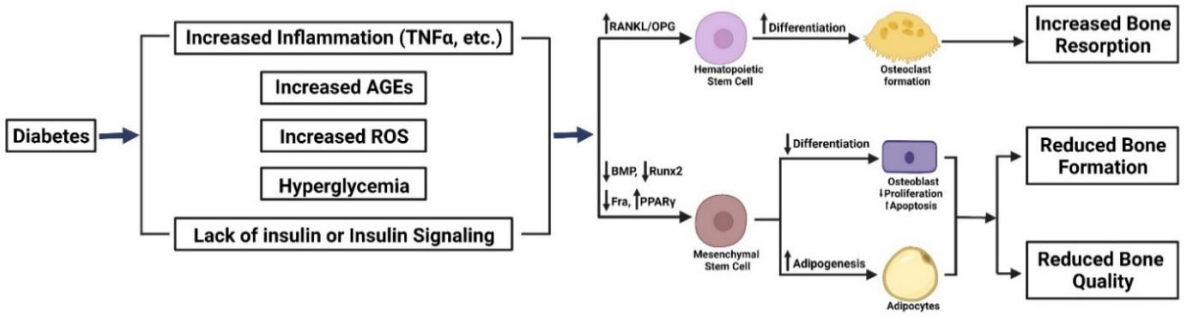

Figure 3: Mechanism of diabetes causing increased osteoclast formation and decreased osteoblast formation [8]; made with Biorender.com.

Skeletal fractures are also a major concern in individuals with CKD. In healthy individuals, elevated phosphorous levels cause osteocytes to produce fibroblast growth factor 23 (FGF23) which increases renal excretion of phosphorous and reduces PTH levels by inhibiting the parathyroid gland. In CKD, the kidney is unable to clear phosphorous effectively. This excess phosphorous level drives the production of FGF23 by promoting the degradation of 1,25-dihydroxivitamin-D (calcitriol), the active form of vitamin-D, to decrease phosphorous levels [17-19]. This results in a net loss of calcium due to decreased absorption from the intestine. Therefore, there is an overall decrease in calcitriol and calcium and increase in phosphorous levels in CKD individuals which all trigger the synthesis of PTH. PTH acts on the kidneys to reduce calcium excretion and increase phosphate excretion while simultaneously stimulating calcitriol production which then increases absorption of intestinal calcium and phosphorus. PTH also increases phosphorous and calcium release from bone reserves to normalize serum levels. Prolonged stimulation of the parathyroid gland to normalize calcium levels leads to hyperplasia and clonal proliferation of parathyroid cells with fewer receptors for vitamin D and calcium. Over the progression of the disease, the parathyroid gland becomes unresponsive to these downregulators resulting in grossly elevated levels of PTH leading to hypercalcemia [19].

Animal models of diabetes are frequently utilized and is insightful to understanding the pathophysiology of the disease state. In particular, we are interested in a mouse model of type-2-diabetes that accurately mimics the hyperglycemia, hyperinsulinemia, insulin resistance and β-cell dysfunction that is quintessential of T2D, while also imitating the multiorgan and skeletal deteriorations of the disease state [2, 3]. The diagnosis of diabetes mellitus in humans is defined by fasting blood glucose levels that are greater than 126 mg/dL or non-fasting blood glucose levels

exceeding 200 mg/dL. Glycated hemoglobin (HbA1c) levels greater than 6.5% or blood-glucose levels greater than 200 mg/dL two hours after a glucose tolerance test also indicates that an individual has diabetes [20, 21]. However, these set criteria for humans are not directly interchangeable with mice as the baseline blood glucose in healthy mice are higher in comparison. In studies using mouse models, blood glucose levels surpassing 300 mg/dL is a common classification criteria for diabetes in mice [22, 23]. There are several mouse models to study the disease mechanism of T2D.

Table 1: Type-2-diabetes mouse models

Mouse Strain		Details
Diet-Induced	C57BL/6J	Mouse were fed a high-fat diet. Mouse become obese however, the fasting blood glucose levels usually plateau around 200 mg/dL and mouse never develop diabetes [24].
Monogenic mutation model	MKR	By introducing a point mutation to insulin-like growth factor 1 receptor (IGF-1R) in the skeletal muscles, the muscle IGF-1R–lysine-arginine (MKR) mouse model. The MKR mouse model is a lean model of T2D and mice become diabetic by 7-8 weeks [24].
	ob/ob	An inactivating mutation to the leptin gene results in obesity, insulin resistance, hyperinsulinemia and hyperphagia in mice as early as 3 weeks. Within 12-20 weeks of age, mice develop diabetes with blood glucose levels reaching as high as 400 mg/dL. However, as the mice get older blood glucose levels start to reach back to normal levels [24].
	db/db	In the db/db mouse model, the leptin receptor has a mutation which induces a severe diabetic phenotype. Within 4 weeks of age, mice develop obesity, insulin resistance, hyperinsulinemia, and hyperphagic. By 12wks of age, the blood glucose levels peak at 400 mg/dL [24].
Polygenic mutation models	KK	The Kuo Kondo (KK) mouse is a moderate obesity model with polygenic mutations. The diabetic state of these mice is dependent on body weight and only the more obese mice develop diabetes [25].
	KK/A^y	The KK/A^y mouse model was produced by introducing the agoti gene to the KK mice. By 8 weeks of age, mice become obese, diabetic, hyperinsulinemic and insulin resistant. Mice maintain their diabetic state with aging, and no dietary supplements are required [24].
	TallyHo	To develop this model, SWR mice were first inbred and then selectively outbred with Thelier Original mice with spontaneous development of hyperinsulinemia and hyperglycemia. The TallyHo mouse model mimics an early onset for T2D but only in male mice [24].
	M16	Mice were selectively bred long-term to develop a polygenic mutation model that develops obesity by 3 to 6 weeks of age. Neither male nor female mice develop diabetes [24].
	NSY	By selectively breeding mice that have elevated blood glucose levels and hyperinsulinemia, the Nagoya-Shibata-Yasuda (NSY) mouse model was developed. Even though mice become mildly obese and hyperinsulinemic, they never develop diabetes [24].
	TSOD	Tsumura Suzuki Obese Diabetes (TSOD) mouse model were developed by selectively inbreeding obese mice. Mice develop insulin resistance and have impaired glucose tolerance, but fasting glucose levels never surpass a diabetic state [24].
	NZO	The New Zealand Obese (NZO) is developed by selectively breeding mice with an agouti coat color. Mice develop hyperphagia, obesity and glucose intolerance, but only 50% of male mice develop diabetes [24].

In T2D, approximately 86% of the patients are obese and 50% show signs of chronic kidney disease [4, 9]. Therefore, we wanted to select an obese mouse model of T2D that also captures the kidney dysfunction that is prevalent in T2D. Of those available, only the KK/A^y and db/db obese mouse model develop diabetes in both male and female mice and maintain a diabetic state even as the animals age [24]. Leptin is known to influence bone metabolism, and therefore it would be a compounding factor in any skeletal effects in the db/db model and it would be difficult to attribute the changes solely to the disease state. The KK/A^y mouse model spontaneously develops both obesity and diabetic nephropathy [24]. Therefore, we decided to use the KK/A^y mouse model as it is mimics both the obesity and kidney dysfunction that are typically seen in type-2 diabetic patients.

Developed in 1957 in Nagoya University in Nagoya, Japan, the Kuo Kondo mouse model is a polygenic mutation model whose complete mutation profile is not known [25, 26]. These KK mouse develops mild obesity, glucose intolerance and insulin resistance, and only develops diabetes when on a high fat diet. Furthermore, it was noted that the diabetic state of the KK mouse was body mass dependent with the more obese mice having more a more severe diabetic state. Therefore, to have more consistent genetically obese KK mice, the yellow obesity gene was introduced to create KK/A^y mouse model of type 2 diabetes [25]. The agouti allele controls the production of melanin and gives mice their coat color. Normally, the agouti allele is only expressed in hair follicles but mutations in the gene can cause ectopic expression in other tissues, including adipose tissue, causing obesity in mice [27]. Mutations to the agouti allele (A^y) that create a yellow coat phenotype in mice are dominant over the wild-type allele (a) that produces a black coat. Mice that are homozygous dominant (A^y/A^y) do not develop into viable embryos. Mice heterozygous for the gene (A^y/a) develop obesity and diabetes, and mice with the wild-type allele (a/a)[28].

In this study, we first characterized the metabolic phenotype of the KK/A^y mouse model for T2D. Secondly, we investigated if the KK/A^y mouse model had signs of kidney dysfunction. Lastly, we investigated the skeletal phenotype of the KK/A^y mice.

2. MATERIAL AND METHODS

2.1 Animals and Treatment

Male and female mice were obtained from Jackson Laboratory with approval from the School of Science Institutional Animal Care and Use committee (IACUC) at Indiana University-Purdue University Indianapolis (IUPUI). Heterozygous male and female mice (n=20/grp) were used as the experimental group (KK/A^y), and wild-type male and female mice (n=20/grp) were used as the control (CON). Mice were fed LabDiet 5LG4, a standard laboratory chow, until euthanization at 18 weeks of age via cardiac exsanguination, followed by cervical dislocation. Approximately 1mL of blood was collected per mouse – half of the blood was stored in EDTA tubes at –80ºC and the remainder was centrifuged to obtain the serum which was then stored at –20ºC. The pancreas and kidneys from each mouse were harvested and weighed, then stored in 10% formalin for 24 hours after which they were transferred into 70% ethanol and stored for histology. Tibiae were harvested, stripped of soft tissue, wrapped in phosphate-buffered saline (PBS)-gauze soaked, and stored at –20ºC.

2.2 Body Mass and Blood Glucose Measurements

Body masses and blood glucose measurements were obtained at the same time every week to minimize variability. To quantify blood glucose, no more than 1mm of the tail of each mouse was snipped and a small sample of blood was obtained and measured on an AlphaTRAK2 glucometer (Zoetis, Parsippany, NJ, USA) using setting "dog code – 1". Mice with blood glucose levels greater than 300 mg/dL for two consecutive were considered diabetic.

2.3 Glucose and Insulin Tolerance Testing

Two distinct sets of 6 mice per group were selected using a random number generator and subjected to glucose tolerance testing (GTT) or insulin tolerance testing (ITT) at 17 wks of age, one week prior to the study endpoint. For GTT, mice were fasted overnight for approximately 16 hours. During the test, the fasted mice were injected with a bolus of glucose solution of 4µL per gram of body mass. Blood glucose measurements were then obtained using AlphTRAK2 glucometer at 0, 10, 20, 30, 60 and 90 minutes following the injection of glucose. For ITT, mice

were fasted for approximately 2 hours prior to the test. Regular human insulin Humulin-R (Eli Lilly, Indianapolis, IN, USA) was injected at 3μL per gram of body mass (0.75 U/kg). Blood glucose measurements were then obtained using the same AlphaTRAK2 glucometer at 0, 15, 30, 45 and 60 minutes following the administration of insulin.

2.4 Pancreatic Analysis for Beta-cell Mass

For β-cell mass analysis (n=10/grp), the pancreas samples sectioned, stained, and imaged by the Translation Core, and the Islet and Physiology Core in the Center for Diabetes and Metabolic Diseases at IUPUI. Each pancreas sample was sectioned using a rotary microtome and two slides each were created from 4 equidistant regions 200 μm apart. The slides were then incubated overnight at 4 ºC with anti-insulin (C27C9) rabbit monoclonal antibodies (Cell Signaling Technology, Danvers, MA, USA). To visualize the insulin, anti-rabbit ImPRESS reagent and NovaRed substrate kit were used with hematoxylin for counterstaining. The stained slides were scanned using Zen Blue software (Zeiss, Obserkochen, Germany) to visualize islet cell areas, and analysis was performed via a custom MATLAB code. The islet cell area was then divided by total pancreas area to obtain percent beta-cell mass.

2.5 Blood Biochemistries

Glycated hemoglobin (HbA1c) (n=10/grp) was measured using a Daytona Clinical Chemistry Analyzer that utilizes a latex agglutination inhibition assay, and serum creatinine was measured using a colorimetric assay (Randox Laboratories, Crumlin, UK). Serum insulin (n=10/grp) was obtained using a mouse insulin ELISA kit (Mercodia, Uppsala, Sweden) that uses a direct sandwich technique. Parathyroid Hormone concentration (n=15/grp) was measured using a Mouse PTH 1-84 ELISA kit (Immunotopics Quidel, San Diego, CA, USA). For calcium and phosphorous concentration, a colorimetric assay was used (Pointe Scientific, Canton, MI, USA). Blood Urea Nitrogen was also measured using a urea kit that utilizes a colorimetric assay (BioAssay Systems, Hayward CA, USA).

2.6 Microcomputed Tomography (µCT) and Architectural Analysis

Left tibiae (n=80) were scanned at 8-micron resolution (Skyscan 1172, Bruker, Kontich, Belgium) using 0.7-degree angle increments, two frames averaged and a 0.5mm Al filter (V=60kV, I=167µA). Tibiae were scanned three at a time using a 3-bone-holder [28]. Hydroxyapatite phantoms (0.25 and 0.75g/cm3 CaHA) were used to calibrate bone mineral density during analysis. Images were reconstructed using NRecon software and each bone was rotated consistently using Data Viewer. A 1 mm trabecular region of interest (ROI) was selected beginning just distal to the proximal growth plate, and was segmented from surrounding cortical bone using CTan. This ROI was then used to obtain bone volume fraction (BV/TV), trabecular number (Tb.N), trabecular separation (Tb.Sp), trabecular thickness (Tb.Th) and tissue mineral density (TMD). Cortical properties were determined at 50% of the length of the tibiae. Using CTAn, 1 mm cortical ROI was selected and a custom MATLAB code was used to determine total cross-sectional area (TA), bone area (BA), marrow area, bone area fraction (BA/TA), cortical thickness (Ct. Th), moments of inertia along the minor (Imin) and major (Imax) axes , and cortical TMD. Imin and Imax are the moments of inertia in the the directions of the greatest and least bending resistance, respectively.

2.7 Four-point Bending Mechanical Testing to Failure

Following microCt scanning, left tibiae were tested in a 4-point bending configuration (n=12/grp) with a 9.20 mm support span and 3.10 mm loading span (medial surface in tension) using a 10 lb load cell (Electroforce 5500, TA Instruments, New Castle, DE). The sample were thawed to room temperature and hydrated with PBS, then subjected to a displacement-controlled test to failure at 0.025 mm/s. The force and the displacement profile was recorded for each bone. A custom MATLAB code was used to plot force-displacement curves from which yield force, ultimate force, displacement at yield, post-yield displacement, and total displacement were obtained. The stiffness of each bone was equivalent to the slope of the linear region of the force-displacement curve, and the area under the curve provided the work to yield, postyield work, and total work. Force-displacement data were transformed into stress-strain using standard engineering beam bending equations and values along microCT data at the site of fracture. This curve was used to obtain the yield stress, ultimate stress, strain to yield, and total strain. The elastic modulus was

equivalent to the slope of the linear region of the stress-strain curve and the area under this curve is resilience (to yield) and toughness (to failure) of the material.

2.8 Statistical Analysis

Statistical analysis was performed using GraphPad Prism (GraphPad v9, San Diego, CA). Two-Way ANOVA was first used to compare and analyze the effects of sex and genotype with a significance level at 0.05. In case of no significant interaction, only the main effects were reported. If significant interaction was noted following a 2-way ANOVA, Tukey's post-hoc analysis was completed.

3. RESULTS

3.1 Body Mass and Weekly Blood Glucose Measurements

Body mass for all animals increased throughout the period of the study. Both male and female mice had higher body weights compared to C57BL/6J animals at 17 week of age (males 32.8±2.6g, females 24.1±2.5g) [29]. Blood glucose for KK/A^y animals trended higher than respective controls in both males and females throughout the study period. Around 11 weeks of age, the blood glucose values for the control males showed an upward trend and crossed the diabetic threshold, but the female CON mice remained in the normal range for the duration of the study. (**Fig. 4B**). The body weight of KK/A^y females trended higher than the other groups throughout the study duration (**Fig 4A**). Statistical analysis of average body mass at the study endpoint revealed that KK/A^y females had the highest average body mass when compared to the other three groups (**Fig. 4C**). There was significant interaction for average body mass and blood glucose for the endpoint measures at 17 weeks of age (body mass $p<0.0001$, blood glucose $p<0.0001$). Posthoc analysis showed that there were no differences in body weight or blood glucose between male controls and KK/A^y animals. Female control animals had normal blood glucose levels throughout the study and blood glucose averages were significantly lower in female controls compared to female KK/A^y ($p<0.0001$), male controls ($p<0.0001$) and male KK/A^y ($p<0.0001$) (**Fig. 4D**).

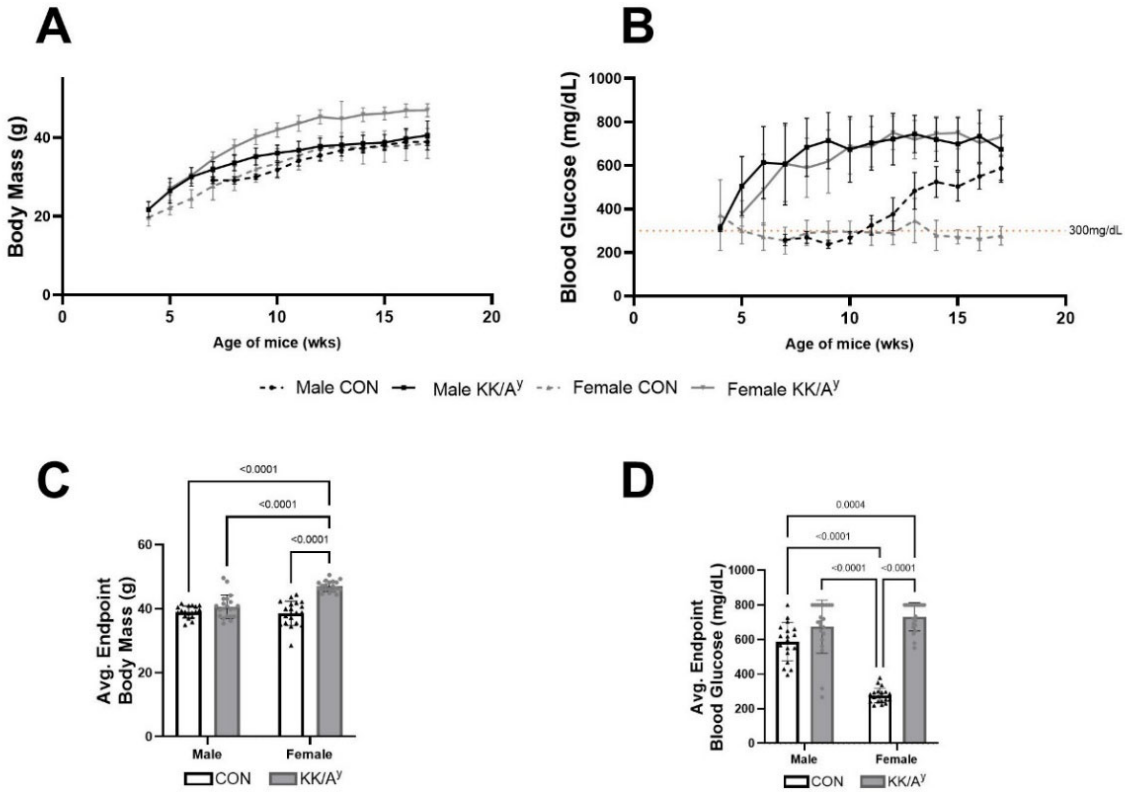

Figure 4: (A) Body masses over the timeline of the study (**B)** Blood Glucose values over the timeline of the study **(C)** Average body mass in 17-week-old mice – graph shows p-values from post-hoc analysis (interaction genotype*sex; p<0.0001 **(D)** Average blood glucose levels in 17-week-old mice – graph shows p-values from post-hoc analysis (interaction genotype*sex; p<0.0001.

3.2 Tibial Length

The tibiae were shorter in KK/A^y animals compared to controls (p=0.0019), and there were no differences in tibial length between the two sexes (**Fig. 5**).

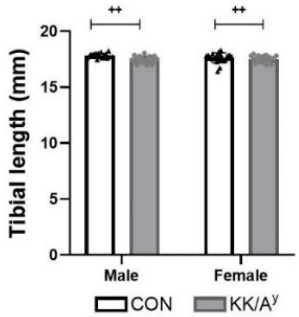

Figure 5: Tibial length obtained after harvest – main effect of genotype (KK/A^y<CON; ++ indicates p=0.0019).

3.3 Soft Tissue Mass

The mass of both the right and left kidneys were higher in males compared to females and higher for KK/A^y animals compared to controls (**Fig. 6A, 6B**). Post-hoc analysis showed that the mass of the pancreas was higher in KK/A^y female mice compared to CON (**Fig. 6C**).

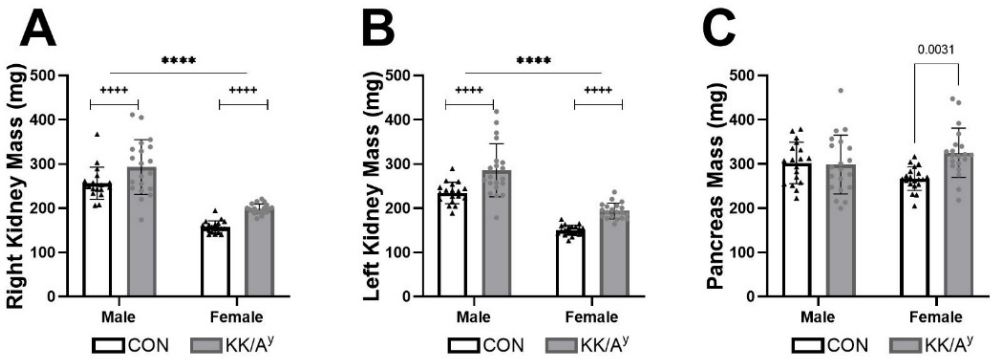

Figure 6: (A) Right kidney mass during harvest – main effects of genotype (KK/A^y> CON; ++++ indicates p<0.0001) and main effects of sex (males>females; **** indicates p<0.0001 (**B)** Left kidney mass during harvest – main effects of genotype (KK/A^y> CON; ++++ indicates p<0.0001) and main effects of sex (males>females; **** indicates p<0.0001) **(C)** Pancreas mass during harvest – graph shows p-values from post-hoc analysis (interaction genotype*sex; p=0.0092).

3.4 Glucose Tolerance Test

The average blood glucose values for all groups were in the normal range following a 16-hour fasting period prior to GTT. Ten minutes after the bolus of glucose was administered, the average blood glucose levels for all animals were above the normal range. By the end of the glucose tolerance test at 120 minutes, only female control animals had blood glucose levels back within the normal range (**Fig. 7A**). The blood glucose values for GTT were normalized by subtracting the fasting blood glucose values at t=0 from their respective group for each time point. The normalized values were then used for AUC plots (**Fig. 7B**). There was a significant interaction between sex and genotype for AUC of GTT (p=0.0128). Posthoc testing revealed that that AUC for CON females was lower compared to KK/A^y females (p=0.009) and KK/A^y males.

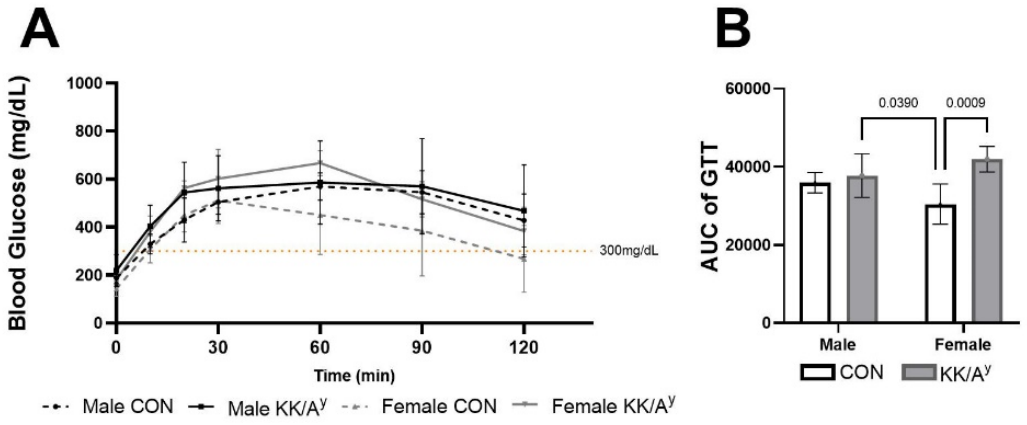

Figure 7: (A) Glucose Tolerance Test at 17wks of age; 300 mg/dL marks the normal range **(B)** Area under the curve for Glucose Tolerance Test –graph shows p-values from post-hoc analysis (interaction genotype*sex; p=0.0128).

3.5 Insulin Tolerance Test

The average blood glucose values for the female control animals were within a normal range following a 2-hour fasting period prior to ITT. After insulin administration, only the female control animals had blood glucose values within the normal range throughout the observation period. The blood glucose values for the male controls increased initially and eventually started to decrease and was approximately back within the normal range at the 45-minute and 60-minute time point. Both male and female KK/A^y animals remained in a hyperglycemic state throughout the observation period (**Fig. 8A**)

The blood glucose values for ITT were normalized by subtracting the fasting blood glucose values from their respective groups for each time point. The signs at each time point was reversed, and the resulting plot was then used for AUC plots (**Fig. 8B**). The AUC was higher for KK/A^y animals compared to controls in females only (p=0.005). For the control animals, the AUC for ITT was significantly elevated for females compared to males (p=0.0189). There were no differences in AUC for ITT between the male control and KK/A^y animals. Compared to the female controls, both male controls (p=0.0189) and male KK/A^y (p=0.0122) had elevated AUC for ITT.

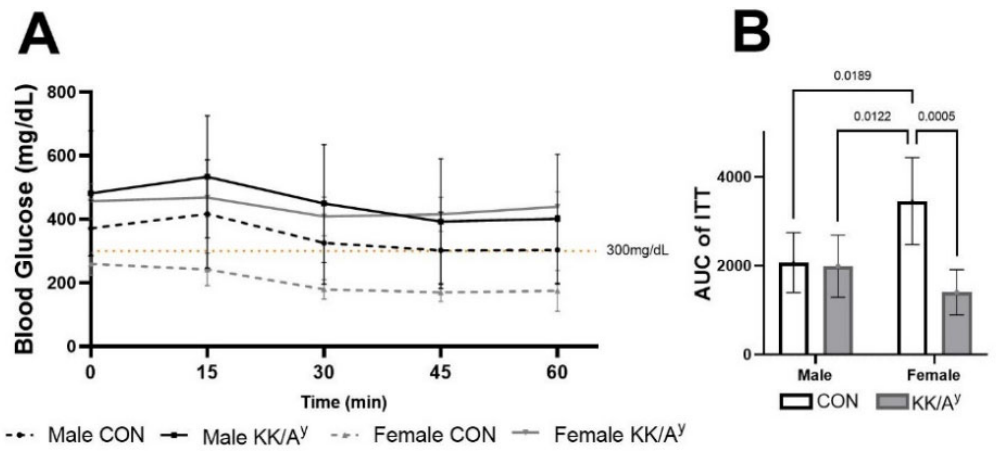

Figure 8: (A) Insulin Tolerance Test at 17 wks of age **(B)** Area under the curve for Insulin Tolerance Test – graph shows p-values from post-hoc analysis (interaction genotype*sex; p=0.0037).

3.6 Blood Measures

In both sexes, the KK/A^y mice had significantly higher HbA1c compared to their respective control groups (males p=0.0069; females p<0.0001). HbA1c was higher in males compared to the females in the control animals (p<0.0001) and there were no differences between males and females for the KK/A^y animals (**Fig. 9A**). KK/A^y females had significantly elevated serum insulin versus controls (p<0.0001), a difference that was not present in males. Control males had higher serum insulin compared to control females (p=0.0062), a trend that flipped for the KK/A^y animals (p=0.0012) (**Fig. 9B**). BUN was significantly elevated in KK/A^y animals from both sexes (main effect of genotype, p=0.0007) (**Fig. 9C**). PTH concentrations were not significantly different between any groups (**Fig. 9D**). The serum concentrations of calcium (**Fig. 9E**), inorganic phosphorous (**Fig. 9F**), and creatinine (**Fig. 9G**) were all elevated in KK/A^y animals compared to CON (main effects of genotype in calcium p=0.0312, inorganic phosphorous p=0.0342, and creatinine p=0.0125).

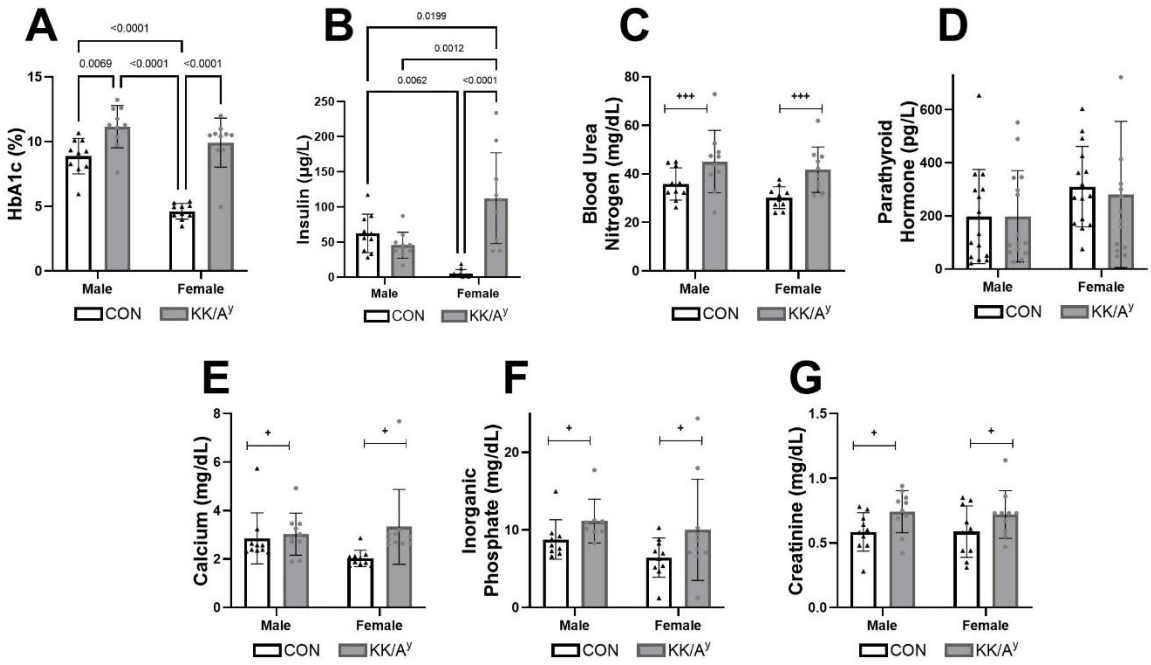

Figure 9: (A) Percent glycated hemoglobin in serum – graph shows p-values from post-hoc analysis (interaction genotype*sex; p=0.0023) **(B)** Serum Insulin Concentration – graph shows p-values from post-hoc analysis (interaction genotype*sex; p<0.0001) **(C)** Serum Blood Urea Nitrogen Concentration – main effects of genotype (KK/Ay> CON; +++ indicates p=0.0007) **(D)** Serum Parathyroid Hormone Concentration **(E)** Serum Calcium Concentration – main effects of genotype (KK/Ay> CON; + indicates p=0.0312) **(F)** Serum Inorganic Phosphate Concentration – main effects of genotype (KK/Ay> CON;+ indicates p=0.0342) **(G)** Serum Inorganic Phosphate Concentration – main effects of genotype (KK/Ay> CON; + indicates p=0.0125).

3.7 Beta-cell Mass

Female KK/A^y mice trended slightly higher than the other three groups, but there were no statistical significance of genotype or sex in beta cell area.

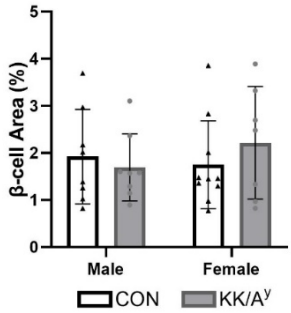

Figure 10: Percent β-cell Area – no significant interactions.

3.8 Trabecular Bone Morphology

Bone volume fraction was higher in KK/A^y mice compared to CON (main effects of genotype, $p<0.0001$), and higher in males compared to females (main effects of sex, $p<0.0001$) (**Fig. 11A**). There was a significant interaction between genotype and sex for trabecular thickness ($p<0.0001$). Trabecular thickness was higher in KK/A^y males compared to CON ($p<0.001$). The CON males had lower trabecular thickness compared to CON females ($p<0.0001$) and the KK/A^y males also had lower trabecular thickness compared to KK/A^y females ($p<0.0001$) (**Fig. 11B**). There was also a significant interaction for trabecular number ($p=0.0054$). KK/Ay females had higher trabecular number versus CON females ($p<0.0001$). Male CON animals had higher trabecular number than female CON ($p<0.0001$), and male KK/A^y animals had higher trabecular number than female KK/A^y animals ($p<0.0001$) (**Fig. 11C**). Trabecular separation was higher in females compared to males (main effects of sex, $p<0.0001$) (**Fig. 11D**). Trabecular TMD was higher in KK/A^y compared to CON (main effect of genotype, $p=0.0024$), and higher in females compared to males (main effects of sex, $p<0.0001$) (**Fig. 11E**).

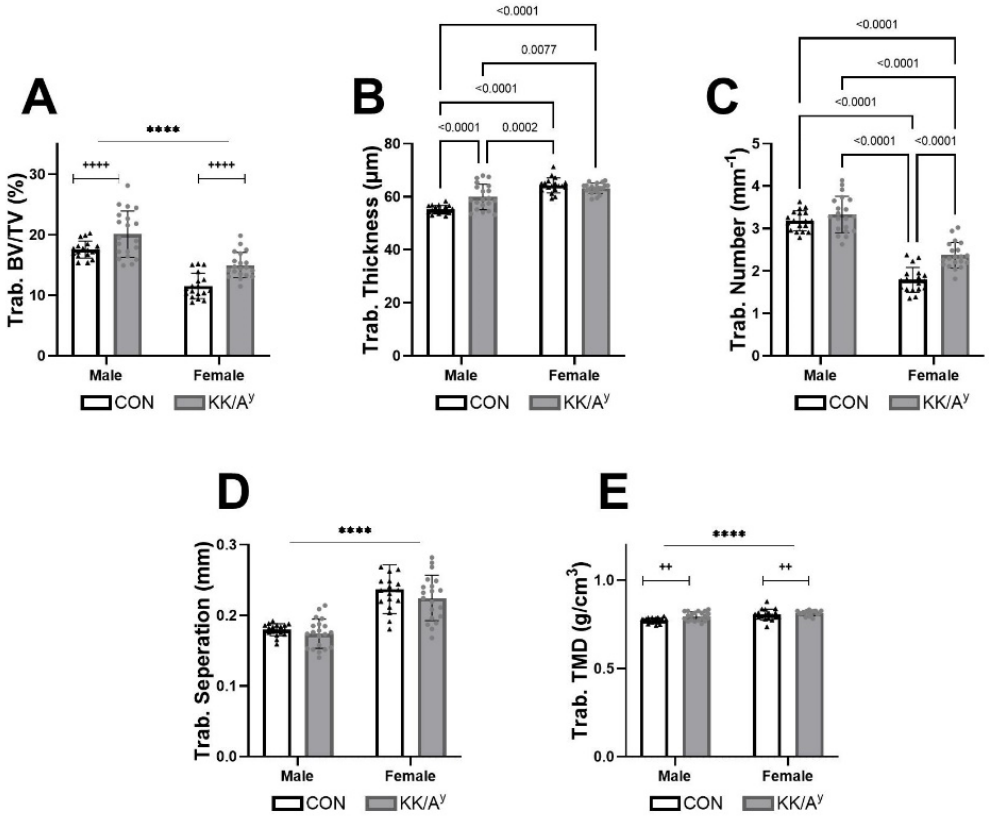

Figure 11: Trabecular Properties **(A)** Bone Volume Fraction – main effects of genotype (KK/A^y> CON; ++++ indicates p<0.0001) and main effects of sex (male>female; **** indicates p<0.0001) **(B)** Trabecular Thickness graph shows – p-values from post-hoc analysis (interaction genotype*sex; p<0.0001) **(C)** Trabecular Number – p-values from post-hoc analysis (interaction genotype*sex; p=0.0054) **(D)** Trabecular Separation – main effects of sex (**** indicates p<0.0001) **(E)** Trabecular Tissue Mineral Density – main effects of genotype (KK/A^y> CON; ++ indicates p = 0.0024) and main effects of sex (male<female; **** indicates p<0.0001).

Table 2: Trabecular Bone Properties

Trabecular Properties	MALE		FEMALE		p-values from 2-way ANOVA		
	CON	KK/A^y	CON	KK/A^y	Genotype	Sex	Interaction
Bone Volume Fraction (%)	17.56 ± 1.40	20.09 ± 3.83	11.54 ± 2.07	14.99 ± 2.10	**<0.0001**	**<0.0001**	0.4333
Trabecular Thickness (µm)	55.18 ± 1.52	59.62 ± 4.81	64.32 ± 2.83	63.20 ± 1.96	**0.0130**	**<0.0001**	**<0.0001**
Trabecular Number (mm^{-1})	3.18 ± 0.24^a	3.33 ± 0.43^b	1.79 ± 0.29^c	2.37 ± 0.30^d	**<0.0001**	**<0.0001**	**0.0054**
Trabecular Separation (mm)	0.18 ± 0.01	0.17 ± 0.02	0.24 ± 0.03	0.22 ± 0.03	0.1363	**<0.0001**	0.5717
Tissue Mineral Density (g/cm^3)	0.77 ± 0.01	0.79 ± 0.03	0.80 ± 0.03	0.81 ± 0.01	**0.0024**	**<0.0001**	0.1078

3.9 Cortical Bone Morphology at the Tibial Midshaft

The total cross-sectional area was higher in males compared to females (main effects of sex, $p<0.0001$) and higher in controls compared to KK/A^y (main effects of genotype, $p=0.0139$) (**Fig. 12A**). There was a significant interaction between genotype and sex for marrow area ($p=0.0112$). KK/A^y males had lower marrow area compared to CON males ($p=0.0151$). The CON males had higher marrow area compared to CON females ($p<0.0001$) and KK/A^y males had higher marrow area compared to KK/A^y females ($p<0.0001$) (**Fig. 12B**). Cortical area was higher in CON animals compared to KK/A^y animals (main effects of genotype, $p=0.0254$) (**Fig. 12C**). There was a significant interaction for bone area fraction ($p=0.0372$). The CON males had lower bone area fraction compared to CON females ($p<0.0001$) and the KK/A^y males had lower area fraction compared to KK/A^y females ($p<0.0001$) (**Fig.12D**). Cortical thickness was higher in females compared to males (main effects of sex, $p<0.0001$) (**Fig. 12E**). The moment of inertia about the minor axis was higher in males compared to females (main effects of sex, $p<0.0001$) (**Fig. 12F**). There was a significant interaction for the moment of inertia (Imax) about the major axis. KK/A^y males had higher Imax compared to CON males ($p=0.0077$). The male CON and KK/A^y animals had higher Imax than female CON and KK/A^y animals respectively (CON, $p<0.0001$; KK/A^y, $p<0.0001$) (**Fig. 12G**). There was a significant interaction for cortical TMD ($p=0.0293$). Cortical TMD for KK/A^y males was higher than CON males ($p=0.0214$), CON females were higher than CON males, and KK/A^y females ($p<0.0001$) were higher than KK/A^y males ($p=0.0002$) (**Fig. 12H**).

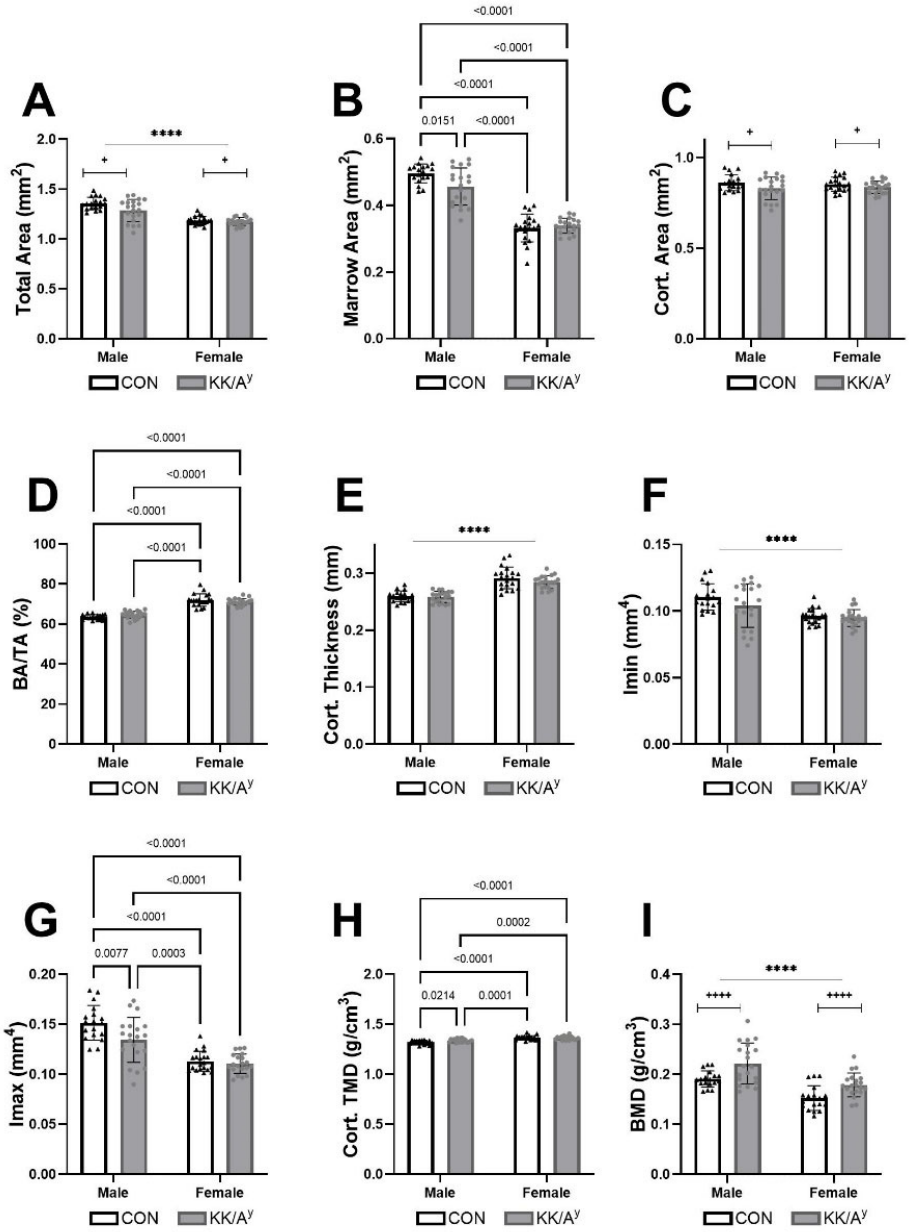

Figure 12: Cortical Properties **(A)** Total Area – main effects of genotype (KK/A^y< CON; + indicates p=0.0139) and main effects of sex (male>female; **** indicates p<0.0001) **(B)** Marrow Area – p-values from post-hoc analysis (interaction genotype*sex; p=0.0112) **(C)** Cortical Area – main effects of genotype (KK/A^y< CON; + indicates p=0.0254) **(D)** Bone Area Fraction – p-values from post-hoc analysis (interaction genotype*sex; p=0.0372) **(E)** Cortical Thickness – main effects of sex (male< female; **** indicates p<0.0001) **(F)** Imin – main effects of sex (male>female; **** indicates p<0.0001) **(G)** Imax – p-values from post-hoc analysis (interaction genotype*sex; p=0.0460) **(H)** Cortical Tissue Mineral Density – p-values from post-hoc analysis (interaction genotype*sex; p=0.0293) **(I)** Bone Mineral Density – main effects of genotype (KK/A^y>CON; ++++ indicates p<0.0001) and main effects of sex (male>females; **** indicates p<0.0001).

Table 3: Cortical Bone Properties

Cortical Properties	MALE		FEMALE		p-values from 2-way ANOVA		
	CON	KK/A^y	CON	KK/A^y	Genotype	Sex	Interaction
Total Area (mm^2)	1.35 ± 0.06	1.29 ± 0.11	1.18 ± 0.04	1.18 ± 0.04	**0.0139**	**<0.0001**	0.0584
Marrow Area (mm^2)	0.49 ± 0.03	0.46 ± 0.06	0.33 ± 0.04	0.04 ± 0.02	0.0744	**<0.0001**	**0.0112**
Cortical Area (mm^2)	0.86 ± 0.04	0.83 ± 0.06	0.85 ± 0.03	0.84 ± 0.02	**0.0254**	0.9038	0.4934
Bone Area Fraction (%)	63.48 ± 1.32	64.64 ± 1.80	72.03 ± 3.11	71.16 ± 1.66	0.7602	**<0.0001**	**0.0372**
Cortical Thickness (mm)	0.26 ± 0.01	0.26 ± 0.01	0.29 ± 0.02	0.28 ± 0.01	0.1748	**<0.0001**	0.2742
Imin (mm^4)	0.11 ± 0.01	0.10 ± 0.02	0.10 ± 0.01	0.09 ± 0.01	0.1037	**<0.0001**	0.2964
Imax (mm^4)	0.15 ± 0.02	0.13 ± 0.02	0.11 ± 0.01	0.11 ± 0.01	**0.0083**	**<0.0001**	**0.0460**
Tissue Mineral Density (g/cm^3)	1.32 ± 0.02	1.34 ± 0.02	1.36 ± 0.02	1.36 ± 0.02	**0.0479**	**<0.0001**	**0.0293**
Bone Mineral Density (g/cm^3)	0.19 ± 0.02	0.22 ± 0.04	0.15 ± 0.02	0.18 ± 0.02	**<0.0001**	**<0.0001**	0.7233

3.10 Structural and Estimated Tissue Level Properties of the Tibia

On a structural level, ultimate force and stiffness were higher in females compared to males (main effects of sex: ultimate force, p=0.0018; stiffness, p<0.0001), and displacement to yield was higher in males compared to females (main effects of sex, p=0.0462). Even though the yield force showed a significant interaction (p=0.0494), post hoc analysis showed no significant differences between the groups (**Table 4**).

The total strain and modulus were higher in females compared to males (main effects of sex: total strain, p=0.0280; modulus, p<0.0001), and yield strain was higher in males compared to females (main effects of sex, p=0.0018). There were significant interactions for yield stress (p=0.0083) and ultimate stress (p=0.0182). Post hoc analysis indicated that female controls were higher than male controls for both yield stress (p=0.0182) and ultimate stress (p=0.0005) (**Table 5**).

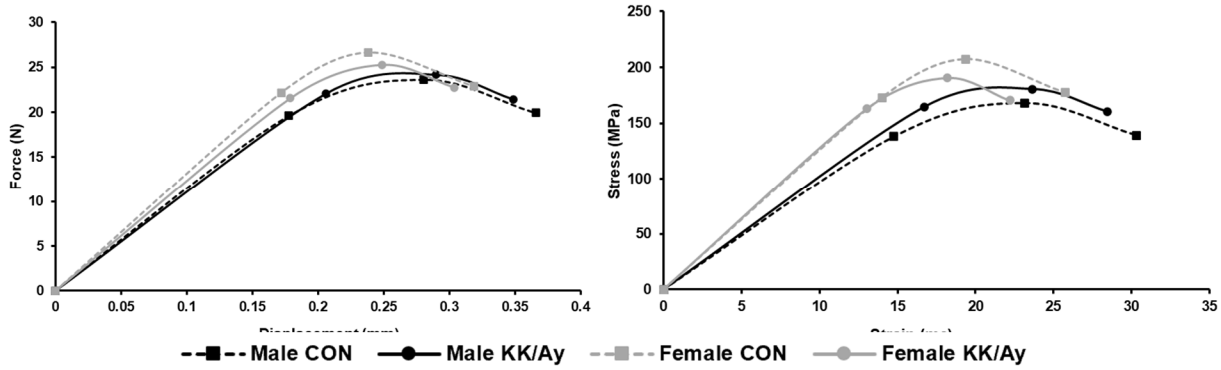

Figure 13: Females trended higher than males in both force vs. displacement curve and stress vs. strain curve.

Table 4: Structural Properties. Yield Force – significant interaction (p=0.0494); posthoc test showed no significant differences between groups

Structural Properties	MALE		FEMALE		p-values from 2-way ANOVA		
	CON	KK/A^y	CON	KK/A^y	Genotype	Sex	Interaction
Yield Force (N)	19.61 ± 2.78	22.01 ± 2.73	22.77 ± 2.82	21.63 ± 3.59	0.4757	0.1194	**0.0494**
Ultimate Force (N)	23.64 ± 3.00	24.16 ± 2.83	27.62 ± 1.74	25.24 ± 2.60	0.2295	**0.0018**	0.0633
Displacement to Yield (mm)	0.18 ± 0.04	0.20 ± 0.02	0.17 ± 0.03	0.18 ± 0.03	0.0597	**0.0462**	0.2616
Post-yield Displacement (mm)	0.23 ± 0.21	0.15 ± 0.09	0.16 ± 0.09	0.13 ± 0.07	0.1247	0.2058	0.4815
Total Displacement (mm)	0.36 ± 0.13	0.35 ± 0.10	0.33 ± 0.07	0.30 ± 0.07	0.4823	0.1284	0.8598
Stiffness (N/mm)	131.0 ± 17.8	124.4 ± 18.8	160.3.0 ± 19.4	145.9 ± 20.9	0.0682	**<0.0001**	0.4852
Work to Yield (mJ)	2.00 ± 0.64	2.47 ± 0.48	2.12 ± 0.57	2.13 ± 0.58	0.1186	0.5011	0.7229
Post-yield Work (mJ)	4.68 ± 3.80	3.26 ± 1.93	3.92 ± 2.03	3.02 ± 1.59	0.1582	0.5393	0.1697
Total Work (mJ)	6.96 ± 3.64	5.72 ± 1.84	6.05 ± 1.70	5.15 ± 1.72	0.1893	0.3926	0.9674

.

Table 5: Tissue Properties. Yield Stress – significant interaction (p=0.0083); posthoc analysis indicated b>a (p=0.0024). Ultimate Stress – significant interaction (p=0.0182); posthoc analysis indicated d>a (p=0.0005). Resilience – significant interaction (p=0.0267); post hoc analysis showed no significant differences between groups.

Tissue Properties	**MALE**		**FEMALE**		**p-values from 2-way ANOVA**		
	CON	**KK/A^y**	**CON**	**KK/A^y**	**Genotype**	**Sex**	**Interaction**
Yield Stress (MPa)	138.1 ± 17.1^a	164.1 ± 26.4	178.8 ± 29.1^b	163.4 ± 28.5	0.4808	**0.0106**	**0.0083**
Ultimate Stress (MPa)	168.1 ± 32.7^c	180.3 ± 28.5	216.5 ± 24.7^d	190.3 ± 19.5	0.3795	**0.0006**	**0.0182**
Yield Strain (mε)	14.77 ± 3.20	16.52 ± 1.73	13.7 ± 2.57	12.87 ± 1.92	0.5284	**0.0018**	0.0721
Total Strain (mε)	30.34 ± 11.10	23.63 ± 7.13	26.4 ± 5.26	22.14 ± 5.12	0.2054	**0.0280**	0.5819
Modulus (GPa)	11.15 ± 1.36	11.37 ± 1.64	15.74 ± 3.34	15.02 ± 1.74	0.6922	**<0.0001**	0.4518
Resilience (MPa)	1.17 ± 0.41	1.50 ± 0.37	1.34 ± 0.37	1.17 ± 0.32	0.4669	0.4775	**0.0267**
Toughness (MPa)	4.07 ± 2.75	3.53 ± 1.34	3.86 ± 1.37	2.82 ± 0.95	0.1301	0.3780	0.6319

4. DISCUSSION

In this study both male and female KK/A^y mice exhibited a diabetic state as evidenced by chronic elevation in blood glucose levels, elevated HbA1c levels, and an inability to reach normal blood glucose levels following a glucose tolerance test or following exogenous insulin administration. Typically, as type-2-diabetes progresses, patients develop insulin resistance triggering insulin overproduction by β-cell which eventually causes β-cell degradation. As disease progression furthers, intensive pharmaceutical interventions and insulin replacement therapy are both required to maintain normoglycemia [30, 31]. The mice have high serum insulin levels and high glucose levels, but in this case the disease state did not affect β-cell mass in these 18-week-old diabetic mice. This indicates that the hyperglycemic state in these mice is primarily due to insulin resistance, and they are appropriately modelling the metabolic phenotype of early stages of type 2 diabetes.

Previous studies using this mouse model showed that the yellow mice with the agouti mutation developed diabetes while the mice with the wild-type agouti gene remained euglycemic, with both groups being overweight [32, 33]. From weekly blood glucose and body mass measured obtained for the duration of the study, we noted that all the animals used in the cohort were obese but only female controls had normal blood glucose values. Male controls were hyperglycemic and were in the diabetic range, defined by blood glucose levels greater than 300 mg/dL. Social isolation in mice increases stress hormone production which could increase blood glucose concentrations [34-36]. Following the death of two male controls due to aggression at 11 weeks of age, a majority of the mice in this group were housed individually, which parallels the sudden rise in blood glucose levels that is observed and may explain their hyperglycemic state. In future studies, mice will be obtained from an in-house breeding colony rather than a commercial source, which should help to minimize the fighting in the male controls.

The KK/A^y mice become diabetic due to insulin resistance, a major driver of T2D progression in humans. This may be crucial in understanding skeletal deterioration with T2D as insulin is typically anabolic to bone[37]. A high-fat diet in C57BL/6J mice causes obesity and impaired glucose tolerance but the animals do not become consistently become diabetic [24]. Other variations of diet-induced T2D studies have attempted to use high fat-diet in combination with streptozotocin (STZ) administration, a compound that is toxic to β-cell and causes apoptosis, to

get the animals to a diabetic state[38, 39]. While this was found to be effective in inducing a diabetic state in mice with mice by decreasing islet cell mass, this method does not capture the insulin resistance which is an important driver in the progression of type 2 diabetes [2, 31, 38, 39]. Other obese mouse models that are prevalent in diabetes studies are the ob/ob and the db/db mouse. These two mice models trigger insulin resistance and obesity in mice via a mutation that affects the leptin gene or leptin receptor. As leptin greatly influences bone metabolism and we aim to study the skeletal impacts of T2D, using either of these models would prevent us from attributing any skeletal changes observed to the disease state alone [24].

Other work has shown that KK/A^y mice have thickening of glomerular capillary walls and develop diabetic nephropathy [24]. In this study, the KK/A^y animals had elevated serum blood urea nitrogen, phosphorus, creatinine, and calcium indicating impaired kidney function and inability to clear waste effectively. Since diabetes is the leading cause of kidney disease, the KK/A^y mouse model of type-2-diabetes affecting kidney function parallels this comorbidity. Future studies using this model will further explore this declining kidney function via urine albumin measures and kidney histology. To manifest the skeletal effects that is common is CKD, an adenine diet may also be used accelerate loss of kidney function or the mice may merely be aged to model a more natural progression of the disease.

Tibial length was greater in the control animals compared to KK/A^y indicating a reduction in longitudinal bone growth. The disease state did not impair trabecular properties, and unexpectedly KK/A^y mice had superior trabecular bone volume fraction and tissue mineral density compared to controls. Skeletal deterioration to bone microarchitecture in diabetic mice caused a reduction in cortical bone area and a less robust bone cross-section at the mid-diaphysis of the tibiae. Sex-specific effects resulted in deterioration to varying skeletal properties in male vs. female mice. KK/A^y females had greater trabecular deteriorations than KK/A^y males in bone volume fraction and trabecular number with increased trabecular separation. In contrast, KK/A^y males suffered greater trabecular deterioration compared to females in tissue mineral density and trabecular thickness. Mechanical properties were only mildly impaired by the disease state with no significant differences although there was a downward trend in both structural and tissue level properties. The prevailing argument is that elevated blood glucose drives the production of AGEs in bone tissue which stiffens the tissue but also makes it fail in a brittle manner. Although AGEs were not measured here, the lack of compelling mechanical changes suggests that either AGEs

formed but were not detrimental, or that additional time is needed for tissue properties to be impacted. Future studies will not only measure the presence of AGEs in bone, but will also extend the timeline to determine when (or if) AGEs form and impact skeletal mechanics. There were several properties that were impacted by animal sex. The female bones were thicker but their overall size a bending resistance (moment of inertia) were reduced. However, tissue level properties were elevated in the females which ultimately translated into bones that were stiffer at the structural. This trend of increased mechanical integrity, especially at the structural level, is not common in mouse models, but the background strain for the model has not often been studies. Future work into the differences in female versus male mice is needed to explore this observation.

A major limitation in this study was the hyperglycemic state of control mice. Chronic elevations of blood glucose in the male control mice, which exceeded 300 mg/dL, would be classified as diabetic per criteria set in the study and used extensively in the literature. Therefore, instead of the comparison being between a diabetic and a non-diabetic state, the comparison reflected differences between a moderate and severe hyperglycemic state. These control mice potentially also had skeletal impairments due to diabetes making the comparison between groups less compelling. Although female control mice did not exceed the diabetic threshold, the average value hovered close for the entire study and many individual mice were, in fact, above the threshold. The fact that control mice were also obese could also have negatively impacted our ability to detect disease-induced differences. Future studies may select a different background strain to serve as a non-obese and non-diabetic control. An additional limitation was that the mice used here were a subset from a larger intervention study where the right limbs were mechanically loaded starting from 13 weeks of age. Although we are characterizing the non-loaded left limbs here, there could have been systemic effects from handling the mice. In addition, the data here will be used as control data for that intervention study.

In conclusion, the study successfully confirmed that the metabolic phenotype of the KK/A^y mice is characteristic of type-2-diabetes, with KK/A^y mice also developing early stages of diabetic nephropathy. The disease state affected cortical microarchitectural properties of bone, but mechanical properties were largely unaffected. Since the mice modeled preliminary stages of type 2 diabetes, using older mice in future studies may allow the disease state to manifest in the skeleton and more accurately mimic the increased fracture prevalence that is typical of type-2-diabetes.

REFERENCES

1. Chatterjee, S., K. Khunti, and M.J. Davies, *Type 2 diabetes.* The lancet, 2017. **389**(10085): p. 2239-2251.
2. Banday, M.Z., A.S. Sameer, and S. Nissar, *Pathophysiology of diabetes: An overview.* Avicenna Journal of Medicine, 2020. **10**(04): p. 174-188.
3. Nowakowska, M., et al., *The comorbidity burden of type 2 diabetes mellitus: patterns, clusters and predictions from a large English primary care cohort.* BMC medicine, 2019. **17**(1): p. 1-10.
4. Daousi, C., et al., *Prevalence of obesity in type 2 diabetes in secondary care: association with cardiovascular risk factors.* Postgraduate medical journal, 2006. **82**(966): p. 280-284.
5. Layden, B., V. Durai, and W. Lowe Jr, *G-protein-coupled receptors, pancreatic islets, and diabetes.* Nature Education, 2010. **3**(9): p. 13.
6. Cohen, R.N., *ENCYCLOPEDIA OF HORMONES—3 VOLUME SET*. 2004, LWW.
7. Galicia-Garcia, U., et al., *Pathophysiology of type 2 diabetes mellitus.* International journal of molecular sciences, 2020. **21**(17): p. 6275.
8. Jiao, H., E. Xiao, and D.T. Graves, *Diabetes and its effect on bone and fracture healing.* Current osteoporosis reports, 2015. **13**(5): p. 327-335.
9. Alicic, R.Z., M.T. Rooney, and K.R. Tuttle, *Diabetic kidney disease: challenges, progress, and possibilities.* Clinical journal of the American Society of Nephrology, 2017. **12**(12): p. 2032-2045.
10. Lv, J.-C. and L.-X. Zhang, *Prevalence and disease burden of chronic kidney disease.* Renal Fibrosis: Mechanisms and Therapies, 2019: p. 3-15.
11. López-Novoa, J.M., et al., *Common pathophysiological mechanisms of chronic kidney disease: therapeutic perspectives.* Pharmacology & therapeutics, 2010. **128**(1): p. 61-81.
12. Baumgarten, M. and T. Gehr, *Chronic kidney disease: detection and evaluation.* American family physician, 2011. **84**(10): p. 1138-1148.
13. Chen, T.K., D.H. Knicely, and M.E. Grams, *Chronic kidney disease diagnosis and management: a review.* Jama, 2019. **322**(13): p. 1294-1304.
14. DeFronzo, R.A., W.B. Reeves, and A.S. Awad, *Pathophysiology of diabetic kidney disease: impact of SGLT2 inhibitors.* Nature Reviews Nephrology, 2021. **17**(5): p. 319-334.

15. Thomas, M.C., et al., *Diabetic kidney disease.* Nature reviews Disease primers, 2015. **1**(1): p. 1-20.

16. Sanches, C.P., A.G.D. Vianna, and F.d.C. Barreto, *The impact of type 2 diabetes on bone metabolism.* Diabetology & Metabolic Syndrome, 2017. **9**(1): p. 1-7.

17. Bacchetta, J., et al., *The consequences of chronic kidney disease on bone metabolism and growth in children.* Nephrology Dialysis Transplantation, 2012. **27**(8): p. 3063-3071.

18. Shimada, T., et al., *FGF-23 is a potent regulator of vitamin D metabolism and phosphate homeostasis.* Journal of bone and mineral research, 2004. **19**(3): p. 429-435.

19. Fish, R.S. and J. Cunningham, *Chronic Kidney Disease-Mineral and Bone Disorder (CKD-MBD)*, in *Primer on Nephrology*. 2022, Springer. p. 1195-1205.

20. Inzucchi, S.E., *Diagnosis of diabetes.* New England Journal of Medicine, 2012. **367**(6): p. 542-550.

21. *Diagnosis*. [cited 2022 7-1-2022]; Available from: https://www.diabetes.org/diabetes/a1c/diagnosis.

22. King, A.J., *The use of animal models in diabetes research.* British journal of pharmacology, 2012. **166**(3): p. 877-894.

23. Leiter, E.H., *Selecting the "right" mouse model for metabolic syndrome and type 2 diabetes research*, in *Type 2 Diabetes*. 2009, Springer. p. 1-17.

24. Fajardo, R.J., et al., *A review of rodent models of type 2 diabetic skeletal fragility.* Journal of Bone and Mineral Research, 2014. **29**(5): p. 1025-1040.

25. Ikeda, H., *KK mouse.* Diabetes research and clinical practice, 1994. **24**: p. S313-S316.

26. DeFronzo, R.A., et al., *Type 2 diabetes mellitus.* Nature reviews Disease primers, 2015. **1**(1): p. 1-22.

27. Moussa, N.M. and K.J. Claycombe, *The yellow mouse obesity syndrome and mechanisms of agouti-induced obesity.* Obesity research, 1999. **7**(5): p. 506-514.

28. *KK.Cg-Ay/J*. [cited 2022 6/30/2022]; Available from: https://www.jax.org/strain/002468.

29. Laboratory, T.J. *BODY WEIGHT INFORMATION FOR C57BL/6J (000664)*. [cited 2022 6/29]; Available from: https://www.jax.org/jax-mice-and-services/strain-data-sheet-pages/body-weight-chart-000664..

30. Fonseca, V.A., *Defining and characterizing the progression of type 2 diabetes.* Diabetes care, 2009. **32**(suppl 2): p. S151-S156.

31. Lebovitz, H.E., *Type 2 diabetes: an overview.* Clinical chemistry, 1999. **45**(8): p. 1339-1345.

32. Hunt, H.B., et al., *Bone tissue collagen maturity and mineral content increase with sustained hyperglycemia in the KK-Ay murine model of type 2 diabetes.* Journal of Bone and Mineral Research, 2018. **33**(5): p. 921-929.

33. Ohnishi, T., et al., *Oxidative stress causes alveolar bone loss in metabolic syndrome model mice with type 2 diabetes.* Journal of periodontal research, 2009. **44**(1): p. 43-51.

34. Kappel, S., P. Hawkins, and M.T. Mendl, *To group or not to group? Good practice for housing male laboratory mice.* Animals, 2017. **7**(12): p. 88.

35. Joëls, M., H. Karst, and R. Sarabdjitsingh, *The stressed brain of humans and rodents.* Acta physiologica, 2018. **223**(2): p. e13066.

36. Ghosal, S., et al., *Mouse handling limits the impact of stress on metabolic endpoints.* Physiology & behavior, 2015. **150**: p. 31-37.

37. Ivaska, K.K., et al., *The effects of acute hyperinsulinemia on bone metabolism.* Endocrine Connections, 2015. **4**(3): p. 155-162.

38. Gilbert, E.R., Z. Fu, and D. Liu, *Development of a nongenetic mouse model of type 2 diabetes.* Experimental diabetes research, 2011. **2011**.

39. Graham, M.L., et al., *The streptozotocin-induced diabetic nude mouse model: differences between animals from different sources.* Comparative medicine, 2011. **61**(4): p. 356-360.